Transmembrane Helix−Helix Association: Relative Stabilities at Low pH†

Neelima Valluru,‡ Frances Silva,‡ Manmath Dhage,‡ Gustavo Rodriguez,‡ Srinivas R. Alloor,‡ and Robert Renthal*,‡,§

Department of Biology, University of Texas at San Antonio, San Antonio, Texas 78249, and Department of Biochemistry, University of Texas Health Science Center at San Antonio, San Antonio, Texas 78229

Received December 11, 2005; Revised Manuscript Received February 19, 2006

ABSTRACT: We have previously studied the unfolding equilibrium of bacterioopsin in a single phase solvent, using Förster mechanism fluorescence resonance energy transfer (FRET) as a probe, from tryptophan donors to a dansyl acceptor. We observed an apparent unfolding transition in bacterioopsin perturbed by increasing ethanol concentrations [Nannepaga et al. (2004) *Biochemistry 43*, 50−59]. We have further investigated this transition and find that the unfolding is pH-dependent. We have now measured the apparent p*K* of acid-induced unfolding of bacterioopsin in 90% ethanol. When the acceptor is on helix B (Lys 41), the apparent p*K* for unfolding is 4.75; on the EF connecting loop (Cys 163), 5.15; and on helix G (Cys 222), 5.75. Five-helix proteolytic fragments are less stable. The apparent unfolding p*K*s are 5.46 for residues 72−248 (Cys 163) and 7.36 for residues 1−166 (Lys 41). When interpreted in terms of a simple equilibrium model for unfolding, the apparent p*K*s give relative free energies of unfolding in the range of −0.54 to −3.5 kcal/mol. The results suggest that the C-terminal helix of bacterioopsin is less stably folded than the N-terminal helices. We analyzed the pairwise helix−helix interaction surfaces of bacteriorhodopsin and three other seven-transmembrane-helix proteins on the basis of crystal structures. The results show that the interaction surfaces are smoother and the helix axis separations are closer in the amino-terminal two-thirds of the proteins compared with the carboxyl-terminal one-third. However, the F helix is important in stabilizing the folded structure, as shown by the instability of the 1−166 fragment. Considering the high-resolution crystal structure of bacteriorhodopsin, there are no obvious helix−helix interactions involving protein side chains which would be destabilized by protonation at the estimated pH of the unfolding transitions. However, a number of helix-bridging water molecules could become protonated, thereby weakening the helix−helix interactions.

In comparison with water-soluble proteins, integral membrane protein folding mechanisms are poorly understood. Results of several folding studies, both in vivo (*1*) and in vitro (*2*−*6*), have been published on membrane proteins containing transmembrane helices. In some in vitro experiments, the membrane proteins were solubilized in detergent micelles, and unfolding was induced by an anionic amphiphile perturbant, dodecyl sulfate. To obtain free energies of unfolding, it is necessary to assume that the free energy changes are linear with perturbant concentration (*7*). Due to nonideal mixing when charged amphiphiles are added to neutral micelles, the assumption of linearity does not necessarily hold (*8*). An alternative approach would be to examine unfolding in a single phase solvent system. We have been studying the unfolding equilibrium of bacterioopsin (BO)[1] in ethanol/water mixtures. We found an apparent unfolding transition in BO perturbed by increasing ethanol concentrations (*9*). However, this measurement was complicated by the p*K* change of the buffer as the solvent composition varied from 0 to 90% ethanol. Thus, the unfolding transition was a composite of solvent-induced and acid-induced unfolding. We have now studied the acid unfolding process by itself, measuring the unfolding equilibria as a function of pH at constant solvent composition. Förster mechanism fluorescence resonance energy transfer (FRET) provides a signal which indicates the folded state. The energy donors are tryptophans, and the energy acceptor is a dansyl group introduced at specific locations in the protein sequence. From these results we are able to obtain relative stabilities of helix−helix interactions in different regions of the protein molecule, suggesting some constraints on possible folding mechanisms.

MATERIALS AND METHODS

Materials. Purple membrane was prepared from *Halobacterium salinarum* (*10*). Wild-type *H. salinarum* was strain

† Supported by a grant from the National Institutes of Health (GM 08194).

* To whom to address correspondence. E-mail: Robert.Renthal@UTSA.edu. Tel: 210-458-5452. Fax: 210-458-4467.

‡ University of Texas at San Antonio.

§ University of Texas Health Science Center at San Antonio.

[1] Abbreviations: BO, bacterioopsin; BR, bacteriorhodopsin; C1, proteolytic fragment of BO containing residues 72−248; C2, proteolytic fragment of BO containing residues 1−71; CHAPS, 3-[(3-cholamidopropyl)dimethylammonio]-1-propanesulfonate; DMPC, dimyristoylphosphatidylcholine; FRET, Förster mechanism fluorescence resonance energy transfer; I222C, BR with isoleucine 222 mutated to cysteine; M163C, BR with methionine 163 mutated to cysteine; TCEP, tris(2-carboxyethyl)phosphine; V1, proteolytic fragment of BO containing residues 1−166; V2, proteolytic fragment of BO containing residues 167−248.

10.1021/bi0525268 CCC: $33.50
Published on Web 03/21/2006

S9, and cysteine mutants (M163C and I222C) were obtained from Janos K. Lanyi, University of California, Irvine. Dansyl chloride, 3-[(3-cholamidopropyl)dimethylammonio]-1-propanesulfonate (CHAPS), and chymotrypsin were obtained from Sigma (St. Louis, MO). *Staphylococcus aureus* V8 protease was obtained from MP Biomedicals (Irvine, CA). Didansyl cystine and tris(2-carboxyethyl)phosphine (TCEP) were obtained from Molecular Probes (Eugene, OR). HPLC grade ethanol was obtained from EMD Chemicals (Gibbstown, NJ). Formic acid (90%) was obtained from J. T. Baker (Phillipsburg, NJ). Sequanal grade trifluoroacetic acid was obtained from Pierce (Rockford, IL). Octyl glucoside was obtained from Calbiochem (La Jolla, CA). Dimyristoylphosphatidylcholine (DMPC) was obtained from Avanti Polar Lipids (Alabaster, AL). Other chemicals were of reagent grade, obtained from standard sources.

Fluorescent Labeling. Purple membrane was reacted with dansyl chloride as previously described (*9*, *11*, *12*). Purple membrane isolated from *H. salinarum* containing single cysteine bacteriorhodopsin (BR) mutants was labeled with didansyl cystine as follows. Purple membrane was suspended in deionized water at 10 μM BR, and 10 μL of 0.1 M TCEP was added. After 30 min at room temperature, the sample was centrifuged at 13000*g*. The supernatant was discarded, and the pellet was resuspended in 0.05 M NaCl and the centrifugation repeated. The pellet was suspended in 0.1 mL of 0.1 M phosphate buffer, pH 8.0, containing 0.1 M NaCl. To this was added 10 μL of 10 mM EDTA and 1.9 mL of 1 mM didansyl cystine in 0.1 M phosphate buffer, pH 8.0, containing 0.1 M NaCl. After reaction for 4 h at room temperature in the dark, the reaction was stopped by adding 0.2 mL of 0.5 M iodoacetamide. After 30 min, the membrane was washed by centrifugation and resuspension in fresh buffer until the supernatant was free of noticeable fluorescence. Fluorescent-labeled purple membrane was lyophilized, solubilized in 90% formic acid, and purified on a column of LH-60. Column solvent was 1:1 $CHCl_3$:methanol containing 0.1 M ammonium acetate. Incorporation of label was estimated by UV spectroscopy (Aviv-Cary 14 spectrophotometer), using an extinction coefficient at 280 nm of 65700 M^{-1} cm^{-1} for bacterioopsin (*13*) and 4500 M^{-1} cm^{-1} for the dansyl group. The stoichiometry was 1 at Lys 41 for dansyl chloride and 0.2 at Cys 163 and 0.8 at Cys 222 for didansyl cystine. Parallel reactions of wild-type BO with didansyl cystine showed no detectable incorporation of fluorescent label. Cleavage of dansyl-Lys 41-BO with *S. aureus* V8 protease and purification of the dansyl-V1 fragment were done as previously described (*13*, *14*). Cleavage with chymotrypsin was done as described by Gerber et al. (*15*), using purple membrane from the M163C mutant. The proteolyzed membrane was then reacted with didansyl cystine, and the dansyl-C1 fragment was purified on LH-60 (*13*). Fluorescent-labeled BO samples (generally 20−30 μM in column solvent) were stored at −20 °C.

Ultrafiltration. Aliquots of fluorescent-labeled BO (0.12 nmol) were dried in a centrifugal evaporator and solubilized in 3 μL of 90% formic acid. The samples were then diluted with 10 μL of ethanol followed by 0.5 mL of 0.1 M ammonium acetate and 40 mM octyl glucoside. Each sample was then concentrated on a Microcon-30 centrifugal concentrator (Millipore, Billerica, MA) at 14000*g* to a volume of approximately 0.1 mL. Each was then diluted with 0.4 mL of 0.1 M ammonium acetate and 40 mM octyl glucoside and again concentrated to about 0.1 mL. The samples were then pooled.

Titrations. Spectrofluorometric titrations were measured on samples containing 0.1 mL of ultrafiltered BO, 0.9 mL of ethanol, and varying amounts of organic acid. In pilot studies, the amount of acid needed to eliminate the sensitized emission signal of ultrafiltered samples was determined. Using this information, a 100 mL sample of 90% ethanol containing 10 mM ammonium acetate was titrated with formic acid and trifluoroacetic acid. A combination glass electrode with a Ag/AgCl reference electrode (Futura 511063; Beckman Coulter, Fullerton, CA) and a Radiometer (Copenhagen, Denmark) PHM 64 pH meter were used to measure pH. The measured pH values determined the amount of acid needed to obtain a particular pH in the 1.0 mL fluorescence spectroscopy samples. The pH was not corrected for the junction potentials in 90% ethanol. However, the correction would be a constant offset applied to all pH values (*16*). The symbol pH* is used to indicate that the measured pH values are correct relative to one another, but the absolute pH is not known. The maximum volume of acid added to 1.0 mL, for the lowest pH samples, was 50 μL of 9% formic acid and 11 μL of 10% trifluoroacetic acid. Fluorescence excitation spectra were measured on a Photon Technology, Inc. (Lawrenceville, NJ), QuantaMaster QM4. The sensitized emission at 490 nm from 285 nm excitation was normalized to the 490 nm emission from 340 nm direct excitation of dansyl. The emission vs pH* data were fit to a titration curve, assuming the titration of a single type of noninteracting group linked to unfolding.

Proteolytic Fragment Association. Dansyl-Lys 41-V1 in 0.2% sodium dodecyl sulfate and 0.05 M phosphate, pH 6.0, was mixed with varying amounts of V2 in the same buffer and then added to CHAPS/DMPC, as previously described for C1 and C2 (*9*).

Computation of Transmembrane Helix Surface Properties. Surface roughness of transmembrane helices was calculated as described previously (*17*). The minimum axial distances of helix pairs were calculated as follows. The C_α atomic coordinates of each helix were averaged in contiguous groups of four, thus generating a set of points on a line passing through the helix axis. The distances between the sets of points for each pair of helices were calculated, and the minimum distance was selected for each pair.

RESULTS

Effect of pH Changes on the Unfolding Equilibrium of BO in Ethanol. In our previous studies, we used the change in FRET between tryptophan donors (Trp 86 and Trp 182) and a dansyl acceptor on Lys 41 (Figure 1) as a signal for unfolding of BO (*9*). Sensitized emission at the dansyl emission maximum of 490 nm was observed from 285 nm tryptophan excitation in aqueous micelles, but the sensitized emission disappeared in 90% ethanol. The samples were prepared from aliquots of dried protein which had been solubilized in a small amount of 90% formic acid. We showed that the high acetate buffer concentration in the final samples held the pH at 4.6 in water. Although we did not attempt to measure the pH in the nonaqueous solutions, we assumed that the acidity of formate and acetate would be

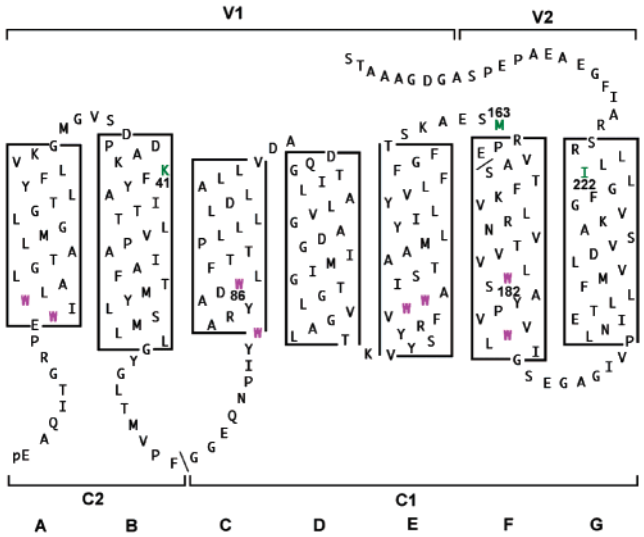

FIGURE 1: Fluorescence resonance energy transfer donors and acceptors. The amino acid sequence of bacterioopsin is shown with α-helices drawn as helical nets. Helices are lettered A−G from the amino to carboxyl terminus. Energy donors and acceptors are numbered by sequence position: predominant tryptophan donors, 86 and 182; dansyl acceptors (attached in separate experiments), 41, 163, or 222. For acceptor attachment to positions 163 and 222, cysteine mutants were used. Proteolytic fragments (C1, V1, and V2) are identified by brackets.

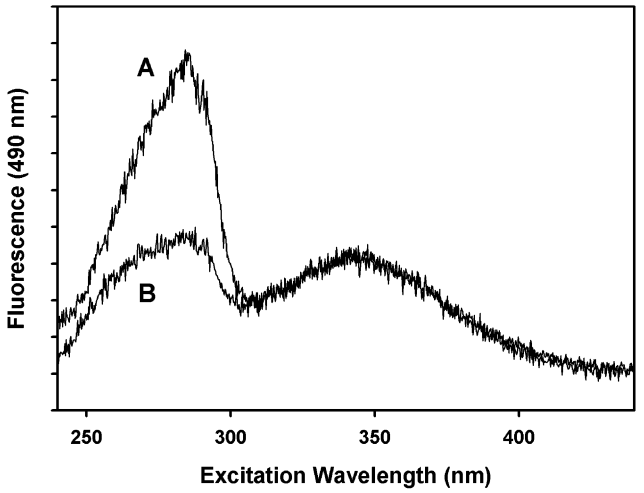

FIGURE 2: Partial unfolding of BO in 90% ethanol. (A) The BO sample was washed on a Microcon-30 ultrafiltration membrane to remove formic acid. (B) BO in 80 mM formic acid. Both samples contained 10 mM ammonium acetate buffer.

similarly diminished by the nonaqueous solvent. However, on further examination we now find that in 90% ethanol, with 0.15 M acetate and 0.07 M formic acid, the acetate almost completely loses its buffering capacity, but the formic acid is mostly dissociated (*18*). Therefore, not only did our protein samples in the previous study undergo a decrease in solvent polarity as the solvent varied between water and 90% ethanol, but there was also an increase in acidity. It is necessary to separate solvent-induced unfolding effects from possible acid-induced unfolding.

We prepared dansyl-Lys 41-labeled BO samples as in the previous study and then washed out the formic acid by ultrafiltration. As shown in Figure 2, curve A, when the formic acid is removed, a large sensitized emission peak is observed at 285 nm, characteristic of folded BO. Curve B

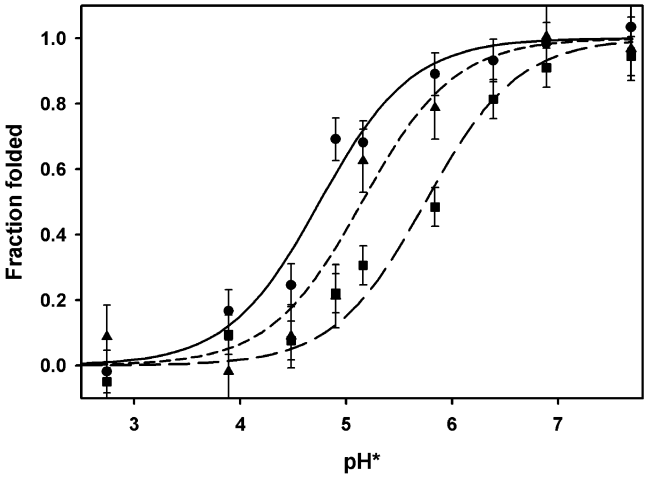

FIGURE 3: Acid-induced unfolding of bacterioopsin. The fraction of folded protein was measured by FRET from tryptophan donors to dansyl acceptors. Acceptors: solid line (circles), dansyl groups on Lys 41 (helix B); short dashed line (triangles), dansyl groups on Cys 163 (EF loop); long dashed line (squares), dansyl groups on Cys 222 (helix G). Conditions: 9:1 ethanol:water (v/v) and 10 mM ammonium acetate; titrated with formic and trifluoroacetic acid. pH*: glass electrode measurements were uncorrected for junction potentials in 90% ethanol. Lines were calculated from p*K*s in Table 1, and error bars indicate standard deviations from lines.

shows an identical sample with 0.08 M formic acid added, demonstrating the low sensitized emission at 285 nm, characteristic of partially unfolded BO. When HCl is added to reach the same value of pH* as in formic acid, the same loss of sensitized emission is observed (data not shown), thus suggesting that the effect is due to acid, not formate. By varying the amount of organic acid added, we obtained a spectrofluorometric titration, as shown in Figure 3, left curve. The data can be fit with an apparent p*K* of 4.75. There is no evidence of cooperativity in the titration, suggesting that there is a single group or class of groups that, when protonated, causes helix B (containing the FRET acceptor) to move away from helix C and helix F (containing the FRET donors). The unfolding reaction is complete within 100 ms, but on a time scale of minutes it is irreversible (S. R. Alloor and R. Renthal, unpublished experiments).

Using BR mutants in which cysteine had been introduced at specific positions, we moved the FRET acceptor location from the B helix to the loop connecting helices E and F (M163C) or to the F helix (I222C). The positions of donors and acceptors in the structure of BR are illustrated schematically in Figure 1. Viewed from the EF connecting loop, the partial unfolding has an apparent p*K* of 5.15 (Figure 3, middle curve). With the acceptor on helix G, the apparent p*K* shifts to 5.75 (Figure 3, right curve). Thus, the stability of the folded structure to acid is different in different regions of the protein.

We also examined the acid-induced unfolding of two different proteolytic fragments of BO, each containing five of the seven BR helices. A chymotrypsin fragment containing residues 72−248 (helices C−G) was purified from BO to which a dansyl group had been attached to Cys 163 (dansyl-Cys 163-C1). The fluorometric titration is shown in Figure 4 (circles). As in Figure 3, the fraction folded was calculated from the intensity of the 285 nm sensitized emission. The data fit a titration curve with an apparent p*K* of 5.46. A *S. aureus* V8 protease fragment containing residues 1−166

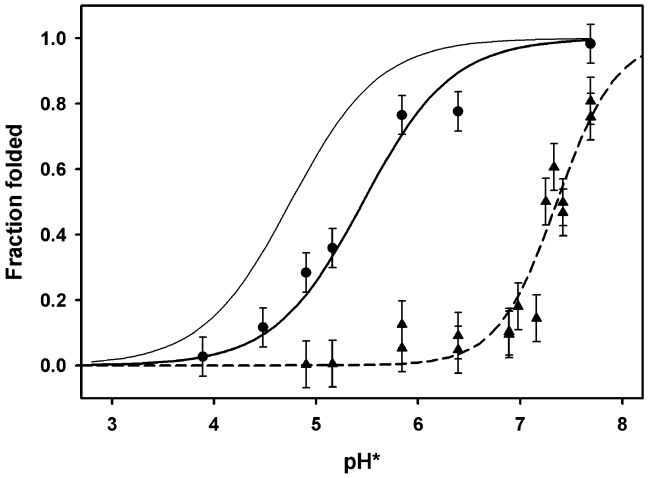

FIGURE 4: Acid-induced unfolding of five-helix fragments of bacterioopsin. The fraction of folded protein was measured by FRET from tryptophan donors to dansyl acceptors. Acceptors: heavy solid line (circles), dansyl groups on Cys 163 (EF loop) of fragment C1 (residues 72−248); dashed line (triangles), dansyl groups on Lys 41 (helix B) of fragment V1 (residues 1−166); thin line, curve fit for the Lys 41 label on intact bacterioopsin (same as solid line in Figure 3). Conditions are the same as in Figure 3.

(helices A−E) was purified from BO to which a dansyl group had been attached to Lys 41 (dansyl-Lys 41-V1). The fluorometric titration is shown in Figure 4 (triangles). The data fit a titration curve with an apparent p*K* of 7.36 and a Hill constant of 1.5. The removal of helices F and G destabilizes the remaining five helices far more than the effect of removing helices A and B. The apparent p*K*s are summarized in Table 1.

Association of V1 and V2 Fragments in Detergent Micelles. The striking instability of the V1 proteolytic fragment of BO led us to examine the interaction of the five-helix V1 fragment with the two-helix V2 fragment. It is known that, in detergent micelles, V1 and V2 spontaneously associate to form BR in the presence of all-*trans*-retinal (*14*, *19*). Also, we previously showed that the proteolytic fragments C1 and C2 interact with an association constant of 7.7×10^6 M^{-1} in the absence of retinal (*9*). To a constant concentration of dansyl-Lys 41-V1 in CHAPS/DMPC micelles, varying amounts of V2 were added. The increase in the sensitized emission at 285 nm due to FRET between Trp 182 and dansyl-Lys 41 was used as a measure of the amount of V1·V2 complex formed. The results are shown in Figure 5. We analyzed the data by a method similar to that reported in Nannepaga et al. (*9*) for the association of proteolytic fragments C1 and C2. By analogy with eq 5 in that paper

$$f_{V1} = [1 + K(V1_T + V2_T) - ((1 + K(V1_T + V2_T))^2 - 4K^2V1_TV2_T)^{0.5}]/2KV1_T \quad (1)$$

where f_{V1} is the fraction of V1 bound to V2, K is the association constant for V1−V2 association, and $V1_T$ and $V2_T$ are the total concentrations of V1 and V2, respectively, in each measurement. As before, we assumed that the maximum sensitized emission measured at 285 nm is that obtained for a BO sample solubilized in CHAPS/DMPC, and the minimum corresponds to the 285 nm emission from V1 alone. We find that the apparent association constant is 0.017 μM^{-1}, much weaker than for association of C1 and C2 (7.7 μM^{-1}; *9*). Both the V1−V2 binding and the acid unfolding results indicate that V1 is partially unfolded in the absence of V2. Thus, V1 unfolds at lower concentrations of acid, and it binds to V2 as if only a small fraction of V1 and/or V2 has the correct conformation for association (see Discussion).

Table 1: pH* Dependence of Acid-Induced Unfolding of BO

protein	FRET acceptor site	modification reaction	apparent p*K*	$\Delta\Delta G_u$ (kcal/mol)
BO	K41	dansyl chloride	4.75	*a*
BO	C163	didansyl cystine	5.15	−0.54
BO	C222	didansyl cystine	5.75	−1.4
C1 fragment	C163	didansyl cystine	5.46	−1.0
V1 fragment	K41	dansyl chloride	7.36	−3.5

[a] Other entries in this column were calculated relative to data for the K41 site in BO using eq 6.

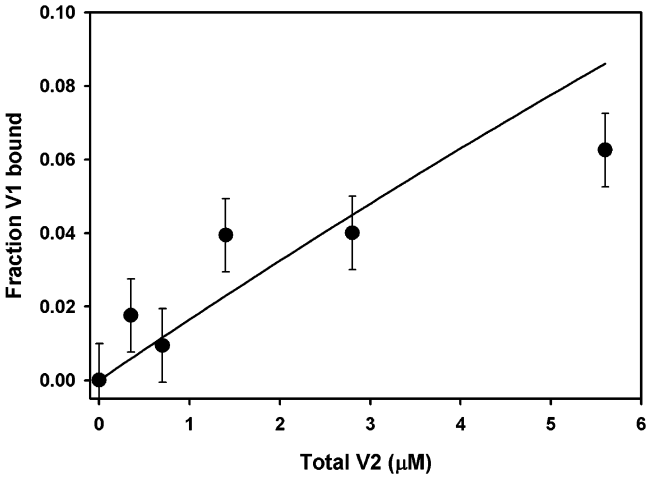

FIGURE 5: Apparent association of V1 and V2 fragments, measured by FRET. V1−V2 association data from the magnitude of the sensitized emission at 285 nm were analyzed as described in the text. The line was calculated from eq 1 with association constant = 0.017 μM^{-1}. Error bars indicate standard deviation from the line. Conditions: 0.7 μM V1, 0.55% CHAPS, 0.55% DMPC, 0.15% SDS, and 0.05 M phosphate, pH 6.0.

Analysis of Helix−Helix Interactions in Seven-Transmembrane-Helix Proteins. The difference in stabilities of different regions of BO to acid or proteolysis prompted us to look at the helix−helix interactions in the structure of BO. The surface roughness of the helix−helix interfaces was measured by calculating the fractal dimension (*17*), and the distance of closest approach was measured between lines fit to the helix axis. The results were plotted in Figure 6. For comparison, the surface roughness and distance of closest approach were also calculated for three other seven-transmembrane-helix proteins. The results indicate that the helix pairs in the N-terminal two-thirds of the proteins have shorter axial distances, and half have smoother interfaces. The helix pairs in the C-terminal one-third of the proteins have longer axial distances and rougher interfaces.

DISCUSSION

Analysis of Acid-Induced Unfolding. Using FRET as an indicator of local conformation, we observed acid-induced unfolding of BO in 90% ethanol (Figure 2), fit by a single p*K*. A simple model can account for the observations. We assume that an unfolding equilibrium is linked with sites

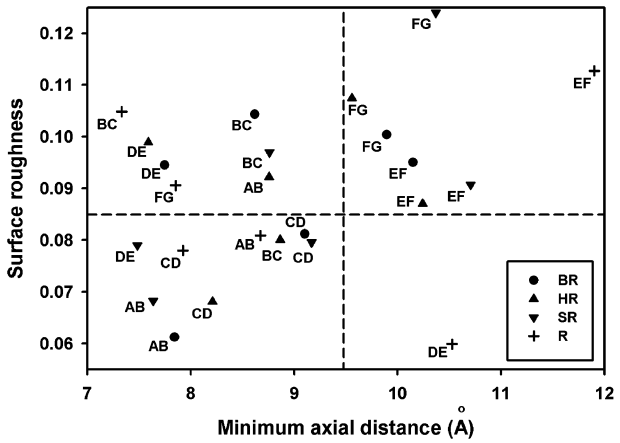

FIGURE 6: Helix−helix interactions in seven-transmembrane-helix proteins. The distance of closest approach of helix pairs was obtained from helix axes by averaging C_α atomic coordinates in contiguous groups of four and then calculating the minimum axial distance. Surface roughness was calculated from the fractal dimension, D (*17*), and plotted as $D - 2$. Protein Data Bank files: circles, BR, 1C3W; triangles, HR (halorhodopsin), 1E12; inverse triangles, SR (sensory rhodopsin II), 1JGJ; crosses, R (bovine rhodopsin), 1F88. Letters next to symbols indicate helix pairs, starting from the N-terminal helix (A) to the C-terminal helix (G).

which have higher p*K*s in the unfolded state of the protein:

$$\begin{array}{ccc} \mathrm{F} & \leftrightarrows & \mathrm{U} \\ \updownarrow & & \updownarrow \\ \mathrm{FH} & \leftrightarrows & \mathrm{UH} \end{array} \qquad (2)$$

where F is the folded protein, U is unfolded protein, UH is unfolded protein protonated at a site which destabilizes the folded form when protonated, and FH is the folded form protonated at the same site. The unfolding equilibrium appears to be established in less than 100 ms, and the analysis which follows refers to this rapid equilibrium. On a time scale of minutes, the reaction is observed to be irreversible. We assume the irreversible step draws equally from folded and unfolded forms, so that the measured fraction of unfolded protein reflects the initial equilibrium concentrations. We define the equilibrium constants for unfolding, sensed by a FRET acceptor at a particular site S on the protein, as $K_S = [U]/[F]$ and $K_S' = [UH]/[FH]$. We assume that a single titrating group or type of group is involved in the equilibria in (2), with a dissociation constant K_a for the equilibrium with U and K_a' for the equilibrium with F. The ratio of the fraction of unfolded protein to the fraction of folded protein f_U/f_F detected by a FRET acceptor at a particular site S will be

$$\begin{aligned}(f_U/f_F)_S &= ([U] + [UH])/([F] + [FH]) = \\ &[U](1 + [H^+]/K_a)/([U]/K_S + [UH]/K_S') = \\ &K_S(1 + [H]/K_a)/\{1 + (K_S/K_S')(1 + [H]/K_a)\} \quad (3)\end{aligned}$$

Since by definition proton binding destabilizes the folded form, it follows that $K_S' > 1 > K_S$ and thus $K_S' \gg K_S$. Therefore, eq 3 reduces to

$$(f_U/f_F)_S = K_S(1 + [H]/K_a) \qquad (4)$$

For a sequential unfolding process, where the protein structure in the region of one FRET acceptor site, S1, is more destabilized by titration of the proton binding site than at another FRET acceptor site, S2, then at a particular pH

$$(f_U/f_F)_{S1}/(f_U/f_F)_{S2} = K_{S1}/K_{S2} \qquad (5)$$

Equation 5 assumes that all side chains with a particular functional group have similar p*K*s when exposed to solvent by unfolding of the protein. We can define the unfolding process at a particular site S as the change in protein conformation which moves the FRET donor/acceptor pairs beyond about 3.5 nm, a distance which would diminish the energy transfer efficiency to a negligible amount for the tryptophan-to-dansyl pair. The free energy change of unfolding at site S, ΔG_u, equals $-RT \ln K_s$. Thus, the difference in unfolding free energy between site S1 and site S2, $\Delta\Delta G_u$, equals

$$\Delta\Delta G_u = -RT \ln[(f_U/f_F)_{S1}/(f_U/f_F)_{S2}] \qquad (6)$$

The results in Figures 2 and 3 were analyzed using eq 6. The acid-induced unfolding of BO viewed from the Lys 41 dansyl site was used as the reference (denominator) for each of the other sites and for the two proteolytic fragments. The values of $\Delta\Delta G_u$ obtained were −0.54 kcal/mol for the 163C site, −1.4 kcal/mol for the 222C site, −1.0 kcal/mol for C1, and −3.5 kcal/mol for V1 (Table 1).

The unfolding process which results in a loss of the FRET signal could be due to movement of the acceptor site away from fixed donor sites, movement of the donor sites away from a fixed acceptor site, or both the donors and the acceptor moving. The relative contributions of BO tryptophans to the sensitized emission at 285 nm can be calculated from the high-resolution crystal structure of BR (Table 2), assuming that the folded state in 90% ethanol has a similar structure (see below). The energy transfer efficiency varies depending on the acceptor position. However, for all three acceptor sites, Trp 182 has the largest contribution and Trp 86 the second largest. Because of the closer proximity of Trp 182 to the acceptors at positions 163 and 222, these positions require a larger change in distance during unfolding to decrease the energy transfer. The titration curves fit well to single p*K*s, with no evidence of broadening within the resolution of the data. A single acceptor site would report more than one p*K* if it detected unfolding processes with different apparent p*K*s. Thus, the simplest interpretation is that each acceptor site moves relative to fixed donors. Of the three FRET acceptor sites that we examined, the C-terminal helix (helix G) appears

Table 2: Calculated FRET Donor−Acceptor Transfer Efficiencies

	K41 N_ϵ		M163 C_ϵ		I222 C_γ	
Trp, C_ϵ	R^a	E^b	R	E	R	E
10	41.9	0.02	43.4	0.01	31.6	0.08
12	38.5	0.03	37.0	0.03	25.7	0.23
80	33.0	0.06	38.0	0.03	31.5	0.08
86	26.2	0.21	26.8	0.19	20.3	0.55
137	35.7	0.04	35.5	0.04	35	0.04
138	34.3	0.05	29.4	0.12	27.2	0.17
182	20.3	0.55	17.7	0.74	13.8	0.93
189	33.9	0.05	32.3	0.07	28.1	0.15

[a] Distances (R) in ångstroms from FRET acceptor sites (Lys N_ϵ, Met C_ϵ, or Ile C_γ) to Trp residues (Trp C_ϵ). Data are from PDB file 1C3W. [b] Fluorescence energy transfer efficiency (E) calculated from $E = R_0^6/(R_0^6 + R^6)$ with $R_0 = 21$ Å.

to be least stably associated with the native structure, and helix B is the most stably associated.

Our survey of four seven-transmembrane-helix protein structures (Figure 6) revealed that the three C-terminal helices (E, F, and G) tend to have topologically rougher surfaces and longer axial separations from neighboring helices, implying weaker interactions. This is consistent with the computational unfolding studies for visual rhodopsin (*20*) which show that the C-terminal third of the protein unfolds more readily than the N-terminal two-thirds. Studies of the stability of the individual helical segments of BO showed that peptides with the sequences of helices F and G did not form helices independently in lipid bilayers (*21*), suggesting that these sequences are less stable than helices A−E. Similar studies of the stability of multihelical fragments of BO showed that of eleven fragments tested, containing two to five helices, only the FG helix pair was substantially less folded in mixed lipid micelles than in the native structure (*22*). Hunt et al. (*21*) previously suggested that the stability of the BR N-terminal helices being greater than the C-terminal helices is consistent with a sequential folding model, in which selection constraints on the first helices synthesized would be more stringent than on the last helices, which would have a template of already associated helices with which to interact. However, our results show that the helix B−helix F interaction is stronger than the helix F−helix G interaction. Thus, helix F does not dissociate along with helix G, but rather in the same process which separates helix B from the core structure. An alternative explanation for the lower stability of the C-terminal helices in rhodopsins is that the retinal attachment site is on helix G, and for retinal to enter its binding pocket, helix G may be required to undergo a displacement.

The importance of the F and G helix interactions with the other BO helices for stabilizing the folded structure is dramatically demonstrated by the five-helix V1 fragment, which lacks helices F and G. V1 is unstable in acid (Figure 4), and the interaction between V1 and the two-helix V2 fragment is far weaker (Figure 5) than that between the five-helix C1 fragment (helices C−F) and the two-helix C2 fragment (helices A−B) (*9*). A possible explanation for this weak association is that both V1 and V2 are partially unfolded. V1 contains only one energy donor site (Trp 86), which is on helix C. The energy acceptor is at Lys 41, on helix B. Thus, the helix B−helix C interaction could be mostly intact in V1 (Figure 4), but the other helices may be partially separated, destroying the binding site for V2. Also, V2 itself is likely to be partially unfolded (*22*). The dissociation equilibrium for V1 and V2 can be written to include partially unfolded forms $V1_u$ and $V2_u$:

$$\begin{array}{ccccc} V1{\cdot}V2 & \leftrightarrows & V1 & + & V2 \\ & & \downarrow\uparrow & & \downarrow\uparrow \\ & & V1_u & & V2_u \end{array} \qquad (7)$$

The apparent association constant, K, as measured in Figure 5 and eq 1 is

$$K = [V1{\cdot}V2]/\{[V1][V2](1 + K_1)(1 + K_2)\} \qquad (8)$$

where K_1 and K_2 are the equilibrium constants between the folded and unfolded forms of V1 and V2, respectively. If the association constant K_v for the folded forms of V1 and V2 is $[V1{\cdot}V2]/([V1][V2])$, then the apparent association constant is

$$K = K_v/[(1 + K_1)(1 + K_2)] \qquad (9)$$

If $K_1 \sim K_2 \gg 1$, and if K_v is approximately the same as the association constant between the chymotryptic fragments of BR, C1 and C1 (*9*), then K_1 and K_2 are in the range of about 20, i.e., only about 5% of V1 and V2 is folded into a form that can associate in CHAPS/DMPC.

The free energy differences observed between the different sites include differences in protein−protein interactions and protein−solvent interactions. The latter are likely to be similar for all helices, so that we assume the measured differences (Table 1) mostly involve helix−helix interactions. The magnitudes of $\Delta\Delta G_u$ are in the range expected for a small number of hydrogen bonds. It would be interesting if we could identify candidate helix−helix hydrogen bonds which might be destabilized in acid and thus explain the observed unfolding. To do this, we need to know the nature of the helix−helix hydrogen bonds and also the pH range of the unfolding experiment.

Although our pH measurements were made on a relative scale, we can estimate the absolute pH. Gutbezahl and Grunwald (*23*) calculated junction potentials between aqueous KCl and alcohol/water mixtures. For 80% ethanol, their results suggest a pH of 1.26 units higher than the measured value; and for 100% ethanol, 2.35 units higher. For 100% methanol, Beckers et al. (*16*) report a pH shift due to the junction potential of 2.25 units. The pH* of the midpoints of the unfolding transitions we observed was in the range 5 to 7, suggesting that the transitions occur at absolute pH values above 6. In this range in 90% ethanol, formic acid is mostly dissociated, protein carboxyl groups are mostly protonated, and Arg and Lys side chains would be mostly protonated (*18*, *24*).

We assume that the starting folded state of BO in 90% ethanol resembles the folded structure of BR. This assumption is supported by the efficiency of energy transfer (e.g., Figure 2), which suggests that in neutral 90% ethanol the three dansyl sites are each at approximately the distances from Trp 86 and Trp 182 found in the native structure. Luecke et al. (*25*) list 31 helix−helix H-bonding interactions involving side chains, observed in the 1.55 Å resolution structure of BR. Thirteen of these H-bonds involve Arg or Lys side chains, of which 11 are bonded to backbone carbonyl oxygens and 2 to Tyr OH. It is unlikely that these oxygens would accept protons from the solvent at the pH of our experiments. Thus these H-bonds are unlikely to be disrupted by protonation. An additional 13 H-bonds involve carboxyl side chains, of which 6 are to hydroxyl side chains (Ser, Thr, or Tyr), 4 are to backbone carbonyl or amide groups, 2 are to other carboxyl side chains, and 1 is to a Lys side chain. Of these, the 2 carboxyl−carboxyl hydrogen bonds might be weakened by protonation, but only if they are ionized in the folded state. Finally, there are 5 H-bonds involving nonionizable side chains, of which 4 are to backbone carbonyl oxygens and 1 involves a Tyr−Trp H-bond. None of these H-bonds is likely to become protonated in the unfolded state. However, 11 of the H-bonds identified by Luecke et al. (*25*) involve helix−helix H-bonds mediated by water molecules. Binding of a proton to a water

molecule that is hydrogen-bonded within a folded protein would undoubtedly disrupt H-bonding, either by directly occupying the acceptor lone pair or by a distortion of bond angles due to the more highly polarized H_3O^+. This raises the intriguing possibility that internally bound water molecules provide a source of stabilization for folding of integral membrane proteins into compact structures.

Buried water molecules have been observed in the interiors of several other high-resolution structures of helical transmembrane proteins, including visual rhodopsin (*26*), a glutamate transporter (*27*), halorhodopsin (*28*), and sensory rhodopsin II (*29*). These water molecules bond almost exclusively to the side chains or backbone within α-helix regions. By contrast, buried water molecules in water-soluble proteins frequently bond to polar groups in loops lacking secondary structure (*30*). Studies of water-soluble proteins indicate that buried water molecules stabilize the structure. For example, cytochrome *f* mutations which remove buried water increase the sensitivity to unfolding (*31*). Conversely, when mutagenesis of lysozyme creates cavities into which water binds, about 2 kcal/mol more free energy is required for unfolding compared to lysozyme with empty cavities (*32*). We plan to direct future experiments toward measuring the extent of stabilization provided by the buried water molecules in BR.

ACKNOWLEDGMENT

We thank Janos Lanyi for providing *H. salinarum* cultures containing the M163C and I222C BR mutations.

REFERENCES

1. Hessa, T., Kim, H., Bihlmaier, K., Lundin, C., Boekel, J., Andersson, H., Nilsson, I., White, S. H., and von Heijne, G. (2005) Recognition of transmembrane helices by the endoplasmic reticulum translocon, *Nature 433*, 377−381.
2. Booth, P. J. (2000) Unraveling the folding of bacteriorhodopsin, *Biochim. Biophys. Acta 1460*, 4−14.
3. Lau, F., and Bowie, J. U. (1997) A method for assessing the stability of a membrane protein, *Biochemistry 36*, 5884−5892.
4. Chen, G. Q., and Gouaux, E. (1999) Probing the folding and unfolding of wild-type and mutant forms of bacteriorhodopsin in micellar solutions: evaluation of reversible unfolding conditions, *Biochemistry 38*, 15380−15387.
5. Yohannan, S., Faham, S., Yang, D., Grosfeld, D., Chamberlain, A. K., and Bowie, J. U. (2004) A C_α−H···O hydrogen bond in a membrane protein is not stabilizing, *J. Am. Chem. Soc. 126*, 2284−2285.
6. Janoviak, H., Struckmeier, J., Hubain, M., Kedrov, A., Kessler, M., and Muller, D. J. (2004) Proving the energy landscape of the membrane protein bacteriorhodopsin, *Structure 12*, 871−879.
7. Pace, C. N. (1986) Determination and analysis of urea and guanidine hydrochloride denaturation curves, *Methods Enzymol. 131*, 266−280.
8. Tanford, C. (1980) *The Hydrophobic Effect*, 2nd ed., pp 81−83, Wiley, New York.
9. Nannepaga, S., Gawalapu, R., Velasquez, D., and Renthal, R. (2004) Estimation of helix−helix association free energy from partial unfolding of bacterio-opsin, *Biochemistry 43*, 550−559.
10. Oesterhelt, D., and Stoeckenius, W. (1974) Isolation of the cell membrane of *Halobacterium halobium* and its fractionation into red and purple membrane, *Methods Enzymol. 31*, 667−678.
11. Harris, G., Renthal, R., Tuley, J., and Robinson, N. (1979) Dansylation of bacteriorhodopsin near the retinal attachment site, *Biochem. Biophys. Res. Commun. 91*, 926−931.
12. Renthal, R., Cothran, M., Dawson, N., and Harris, G. (1987) Fluorescent labeling of purple membrane: implications for helix connections, *Biochim. Biophys. Acta 897*, 384−394.
13. Renthal, R., and Haas, P. (1996) Effect of transmembrane helix packing on tryptophan and tyrosine environments in detergent-solubilized bacterio-opsin, *J. Protein Chem. 15*, 281−289.
14. Sigrist, H., Wenger, R. H., Kislig, E., and Wuthrich, M. (1988) Refolding of bacteriorhodopsin. Protease V8 fragmentation and chromophore reconstitution from proteolytic V8 fragments, *Eur. J. Biochem. 177*, 125−133.
15. Gerber, G. E., Anderegg, R. J., Herlihy, W. C., Gray, C. P., Biemann, K., and Khorana, H. G. (1979) Partial primary structure of bacteriorhodopsin: sequencing methods for membrane proteins, *Proc. Natl. Acad. Sci. U.S.A. 76*, 227−231.
16. Beckers, J. L., Ackermans, M. T., and Bocek, P. (2003) Capillary zone electrophoresis in methanol: migration behavior and background electrolytes, *Electrophoresis 24*, 1544−1552.
17. Renthal, R. (1999) Transmembrane and water-soluble helix bundles display reverse patterns of surface roughness, *Biochem. Biophys. Res. Commun. 263*, 714−717.
18. Grunwald, E., and Berkowitz, B. (1951) The measurement and correlation of acid dissociation constants for carboxylic acids in the system ethanol−water. Activity coefficients and empirical activity functions, *J. Am. Chem. Soc. 73*, 4939−4944.
19. Liao, M.-J., Huang, K.-S., and Khorana, H. G. (1984) Regeneration of native bacteriorhodopsin structure from fragments, *J. Biol. Chem. 259*, 4200−4204.
20. Rader, A. J., Anderson, G., Isin, B., Khorana, H. G., Bahar, I., and Klein-Seetharaman, J. (2004) Identification of core amino acids stabilizing rhodopsin, *Proc. Natl. Acad. Sci. U.S.A. 101*, 7246−7251.
21. Hunt, J. F., Earnest, T. N., Bousche, O., Kalghatgi, K., Reilly, K., Horvath, C., Rothschild, K. J., and Engelman, D. M. (1997) A biophysical study of integral membrane protein folding, *Biochemistry 36*, 15156−15176.
22. Luneberg, J., Widmann, M., Dathe, M., and Marti, T. (1998) Secondary structure of bacteriorhodopsin fragments. External sequence constraints specify the conformation of transmembrane helices, *J. Biol. Chem. 273*, 28822−28830.
23. Gutbezahl, B., and Grunwald, E. (1953) The acidity and basicity scale in the system ethanol−water. The evaluation of degenerate activity coefficients for single ions, *J. Am. Chem. Soc. 75*, 565−574.
24. Gutbezahl, B., and Grunwald, E. (1953) The effect of solvent on equilibrium and rate constants. II. The measurement and correlation of acid dissociation constants of anilinium and ammonium salts in the system ethanol−water, *J. Am. Chem. Soc. 75*, 559−565.
25. Luecke, H., Schobert, B., Richter, H. T., Cartailler, J. P., and Lanyi, J. K. (1999) Structure of bacteriorhodopsin at 1.55 Å resolution, *J. Mol. Biol. 291*, 899−911.
26. Okada, T., Fujiyoshi, Y., Silow, M., Navarro, J., Landau, E. M., and Shichida, Y. (2002) Functional role of internal water molecules in rhodopsin revealed by X-ray crystallography, *Proc. Natl. Acad. Sci. U.S.A. 99*, 5982−5987.
27. Yernool, D., Boudker, O., Jin, Y., and Gouaux, E. (2004) Structure of a glutamate transporter from *Pyrococcus horikoshii*, *Nature 431*, 811−818.
28. Kolbe, M., Besir, H., Essen, L.-O., and Oesterhelt, D. (2000) Structure of the light-driven chloride pump halorhodopsin at 1.8 Å resolution, *Science 288*, 1390−1396.
29. Gordeliy, V. I., Labahn, J., Moukhametzianov, R., Efremov, R., Granzin, J., Schlesinger, R., Büldt, G., Savopol, T., Scheidig, A. J., Klare, J. P., and Engelhard, M. (2002) Molecular basis of transmembrane signalling by sensory rhodopsin II-transducer complex, *Nature 419*, 484−487.
30. Park, S., and Saven, J. G. (2005) Statistical and molecular dynamics studies of buried waters in globular proteins, *Proteins 60*, 450−463.
31. Griffin, S., Vitello, A., and Wittung-Stafshede, P. (2002) Buried water molecules contribute to cytochrome f stability, *Arch. Biochem. Biophys. 404*, 335−337.
32. Takano, K., Yamagata, Y., and Yutani, K. (2003) Buried water molecules contribute to the conformational stability of a protein, *Protein Eng. 16*, 5−9.

BI0525268